An Experimental Study of Spatial Variability of Rainfall

ALI TOKAY

Joint Center for Earth Systems Technology, University of Maryland, Baltimore County, and NASA Goddard Space Flight Center, Greenbelt, Maryland

RIGOBERTO J. ROCHE

Water Science of Coupled Aquatic Processes in Ecosystems from Space, Florida International University, Miami, Florida

PAUL G. BASHOR

Computer Sciences Corporation, and NASA Wallops Flight Facility, Wallops Island, Virginia

(Manuscript received 14 February 2013, in final form 29 October 2013)

ABSTRACT

Spatial variability of rainfall was studied through a gauge network on the Delmarva Peninsula. The gauge network consists of 11 dual- or triple-tipping-bucket sites ranging from 1- to 150-km separation distances. The time of the tip (0.254 mm) was recorded to a datalogger, and a continuous dataset was available from all sites for over 5 yr (May 2005–July 2010). A three-parameter exponential function was fitted to the paired correlations and the resultant correlation distance was 8–13 km during summer and 51–85 km during winter. The correlation distances showed pronounced year-to-year variability as being 8–43 km and 13–67 km during spring and autumn, respectively. The airmass convection was the main weather system during summer while nor'easters played an important role during winter. The 30-min integration and two-tip rain/no-rain threshold was selected for the base of this study. The correlation distance increased with longer integration periods and was 17 and 32 km for 30 min and 1 h, respectively.

1. Introduction

Nonuniform beam filling within the instantaneous field of view (IFOV) is one of the key uncertainties of satellite-based precipitation estimates. It results from the combination of variability of the precipitation intensity and coverage within the IFOV. Tokay and Öztürk (2012, hereafter TO12) investigated the variability of rainfall and nonuniform beam filling effects using a dataset of 2 yr of measurements from six dual rain gauges, where the maximum gauge separation distance was 5 km. This maximum separation distance coincided with the approximate diameter of the footprint of the National Aeronautics and Space Administration (NASA) Tropical Rainfall Measuring Mission (TRMM) precipitation radar. The TO12 study was based on rain gauge measurements over a 2-yr span at the NASA Wallops Flight Facility, Wallops Island, Virginia. This rich gauge dataset enabled the study of rainfall over seasonal, 6-month, and annual periods, as well as under different weather systems and different uniformity conditions. The TO12 study pointed out that the variability of rainfall can only be determined within the maximum gauge separation distance.

For microwave imagers, the IFOV at the surface is an ellipse where the major axis is typically larger than 5 km. For the TRMM Microwave Imager (TMI), after the satellite boost in 2001, the minor and major axes, respectively, are 4.7 and 7.7 km at 85 GHz and 40 and 67 km at 10.65 GHz. The Advanced Microwave Scanning Radiometer for Earth Observing Systems (AMSR-E) on board *Aqua*, on the other hand, has IFOVs of 3.5 km × 5.9 km at 89 GHz and 43 km × 75 km at 6.9 GHz. The Special Sensor Microwave Imager/Sounder (SSMIS) on three Defense Meteorological Satellite Program (DMSP) satellites has IFOVs of 13.2 km × 15.5 km at 91.65 GHz

Corresponding author address: Ali Tokay, NASA Goddard Space Flight Center, Code 612.0, Greenbelt, MD 20771.
E-mail: ali.tokay-1@nasa.gov

DOI: 10.1175/JHM-D-13-031.1

© 2014 American Meteorological Society

and 46.5 km × 73.6 km at 19.35 GHz. The upcoming NASA Global Precipitation Measurement (GPM) Microwave Imager (GMI) will have IFOVs of 4.1 km × 6.3 km at 166 GHz and 19.4 km × 32.1 km at 10.65 GHz. It should be noted that the lower frequency channels, which have larger IFOVs, are those that are primarily used to retrieve the precipitation over the oceans.

Precipitation products that combine the precipitation estimates from active radar and passive microwave sensors have also been constructed over resolutions greater than 5 km. The TRMM Multisatellite Precipitation Analysis (TMPA), for instance, is a 3-hourly, 0.25° × 0.25° precipitation product (Huffman et al. 2007). The Climate Prediction Center Morphing Method (CMORPH), on the other hand, is a half-hourly, 8-km (at the equator) resolution precipitation product (Joyce et al. 2004). The Japan Aerospace Exploration Agency (JAXA) Global Satellite Mapping of Precipitation (GSMaP) is another global product, which is hourly at 0.1° resolution (Aonashi et al. 2009).

The spatial variability of rainfall has been mostly studied over domains less than 40 km in linear extent through ground-based and rain gauge networks. The three-parameter exponential function has been frequently employed to determine the correlation distance, which depends on the storm and gauge network characteristics (e.g., TO12, and references therein). Highly variable convective precipitation events are characterized by shorter correlation distances than those for widespread stratiform precipitation. The correlation distances are sensitive to the number and distribution of the gauges. While the close intergauge distances are preferable, logistical challenges dominate the gauge selection site. The correlation distances are also longer for longer gauge and radar integration periods. Habib and Krajewski (2002) used a dense gauge network where the maximum separation distance was 8 km and reported the correlation distance of 4.6 and 2.5 km for light and heavy rain, respectively, at 15-min time integration. The light versus heavy rain was determined through gridded radar pixel rain intensity that was concurrent with gauge observation. If the rain intensity was greater than 10 mm h^{-1}, it was considered as convective, while the stratiform rain occurred at rain intensities less than 10 mm h^{-1}. Gebremichael and Krajewski (2004) conducted a similar study in determining the correlation distance from a gauge network at 5- and 15-min integrations and snapshots of S-band radar rainfall estimates. The radar-based correlation distances were slightly lower than that of the gauge-based study. These two studies were based on 2-month-long field campaigns in central Florida and in the Amazon basin of Brazil. Moreau et al. (2009), on the other hand, used 1-yr observations of X-band radar and a gauge network where the maximum separation distance was 10 km. They found correlation distances of 4.5–6.1 km depending on two different radar rainfall estimates and gauge-based study.

Villarini et al. (2008) conducted a comprehensive study of variability of rainfall over a 6-yr period using 50 rain gauge observations over a basin of approximately 135 km^2 in southwest England, where the gauge separation distances ranged from 0.5 to 15 km. They demonstrated how the correlation distances and the other parameters of a three-parameter exponential function differed from a similar study in Oklahoma (Ciach and Krajewski 2006). In addition to differences in precipitation characteristics, where the latter exhibits heavy convective precipitation, the maximum gauge separation distance was about 4 km and the sample size was 14 months (mostly spring and summer) in the latter study. The Ciach and Krajewski (2006) study used 25 double-gauge stations, and the events with high and low spatial variability resulted in correlation distances of 4.4 and 9.8 km. They also showed that the correlation distances are longer when the rain rate is above 3 mm h^{-1}. TO12 also pointed out that the variability within the TRMM precipitation radar could be higher when the pixel is partially covered by rain, which may occur in the presence of light rain.

Villarini (2010) evaluated the TMPA rain estimate at its finest spatial and temporal scale over the metropolitan area of Rome, Italy. He used gauge rainfall observations over a 4-month period that covered two TMPA pixels where the maximum gauge separation was 25 km. The correlation distance for 3-h gauge totals was 44.7 km when an exponential function is applied to the paired Pearson's correlations. Mandapaka et al. (2009) used the hourly rainfall from the Oklahoma Micronet rain gauge network, where the maximum gauge separation distance was less than 40 km. They found the correlation distance of 40 km using 8 yr of warm-season observations.

The aforementioned studies focused on the spatial variability of rainfall within ground-based radar pixel and satellite footprint space for hydrological applications. The spatial variability of rainfall has also been studied over monthly, seasonal, and yearly periods over a region where the maximum gauge separation distance is around 400 km. Berndtsson (1987) derived cross correlations of daily rainfall from 5 yr of gauge observations in northern Tunisia. There were significant differences in correlations at a given distance between the different months representing differences in rainfall characteristics. Bewket and Conway (2007) looked at the correlation in seasonal and yearly rainfall in 12 stations in northwest Ethiopia based on 18 yr of gauge record.

FIG. 1. A picture of (top) dual and (bottom) triple rain gauge site.

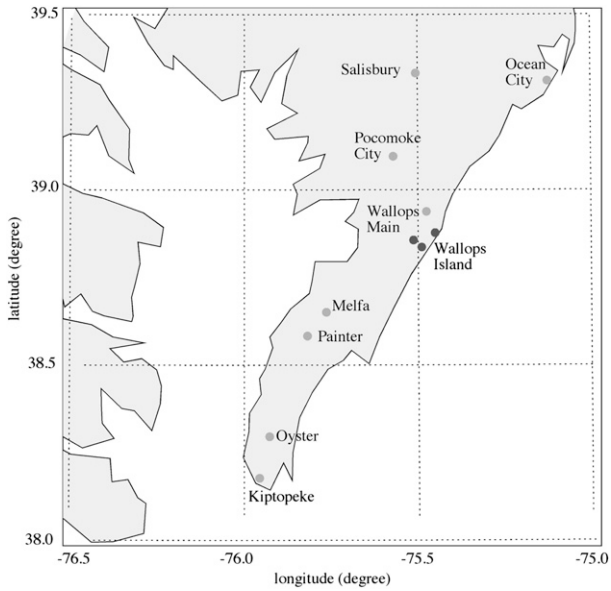

FIG. 2. A map of the Eastern Shore rain gauge network. Triple gauge sites are marked by light gray circles, and dual gauge sites are marked by dark gray circles.

Rainfall was more spatially variable during dry periods than wet periods.

This study addresses the spatial variability of rainfall within the IFOV of the microwave sensors. This study uses a similar methodology and experimental region as the TO12. Nevertheless, the present study employs a much longer dataset than did TO12 and many past studies, which provides a way to examine spatial variability for multiple climatological periods and four different weather systems. Previous studies have relied primarily on field campaign databases and therefore were unable to offer conclusive remarks on the spatial variability caused by a particular weather system. The study area in the present case is also much larger than in the TO12 study and most of the past studies, which is vital in determining the spatial variability within the IFOV of the microwave sensors. The experimental setup and precipitation climatology can be found in sections 2 and 3, respectively, while the data analysis is outlined in section 4. Section 5 demonstrates the spatial variability of rainfall over different time periods. The variability based on specific weather events is also given in section 5. The parameters of exponential fits are given in section 6, followed by concluding remarks in section 7. Future research is presented in section 8.

2. Experimental setup

A dual- or triple-tipping-bucket rain gauge network was deployed on the Delmarva Peninsula, eastern Virginia, and northeast North Carolina in 2004–05 to evaluate NASA's recently modified S-band polarimetric radar. In addition, a dual-tipping-bucket gauge network was deployed at Wallops Island, Virginia, to study the small-scale variability of rainfall (TO12). The former network was also used to evaluate the performance of various operational gauge networks (Tokay et al. 2010). The operation downsized in 2007 because of budgetary limitations where only the gauges on the Delmarva Peninsula continued to operate. This study used eight triple gauge sites from the former and three dual gauge sites from the latter network. A continuous record of gauge observations was available from 15 May 2005 to 31 July 2010 at these 11 sites. The gauges were manufactured by Met One Inc., had a 20.3-cm diameter orifice, and sat on a wooden box (Fig. 1). The time of the tip where each tip corresponds to 0.254 mm of rainfall was recorded on a battery-operated data logger manufactured by MadgeTech Inc.

The gauge network extends from Ocean City, Maryland, to Kiptopeke, Virginia, where the maximum and minimum gauge separation distances are 150 and 1 km, respectively (Fig. 2). The configuration of the gauge sites

allowed at least one pair of gauges for every 10-km increase in gauge separation distance. This is important for the stability of the fitted exponential function. The region is mainly flat and is subject to remnants of tropical cyclones, sea breeze convection, nor'easters, and frontal rainfall.

3. Precipitation climatology

The precipitation amount on the Delmarva Peninsula varies little between seasons. Wallops Island, which resides in the middle of the gauge network, received its maximum amount (274 mm) during summer and minimum amount in autumn (223 mm). At the same time, the region is subject to 2-month-long droughts and abundant rainfall during the passage of tropical cyclones. For the observation period, the minimum precipitation was observed during the winter of 2008/09 and the maximum precipitation occurred during the autumn of 2006, which coincided with the passage of Hurricane Ernesto (2006; Fig. 3a). It should be noted that our precipitation totals in winter months do not include the snow water equivalent, and therefore, the climatology may have higher precipitation in winter months. For the five winter seasons studied here, frozen and mixed precipitation had 13% of total winter precipitation following daily reports from the automated surface observation system weighing bucket precipitation gauge at Wallops Island, Virginia. Winter 2009/10 was subject to high precipitation accumulation events, and therefore, the rainfall exceeded the climatology. Winter 2009/10 had also the highest amount (23%) of nonliquid precipitation among the five winters. The cold-season rainfall totals were less than the climatology, except in 2009/10, while rainfall exceeded the climatology in the warm seasons, except in 2007 (Fig. 3b). The year of 2007/08 was the driest year and the year of 2009/10 was the wettest year (Fig. 3c).

4. Data analysis

Five years of gauge observations have been summed to 10 different rain accumulation periods ranging from 5 min to 12 h. Four different rain/no-rain thresholds were considered ranging from a single tip (0.254 mm) to eight tips (2.032 mm). This study was based on the 30-min rain accumulation period with a two-tip (0.508 mm) rain/no-rain threshold, which resulted in 6870 observations after the snowy days were removed from the dataset. This rich dataset allowed us to study the spatial variability of rainfall for 35 different climatological periods, consisting of 20 seasons, 10 warm/cold periods, and 5 yr. The warm period includes the summer months plus May and September, while the cold period covers the winter months plus November and March. April and October are considered to be transitional periods for this region. Since the rainfall observations started in mid-May, the

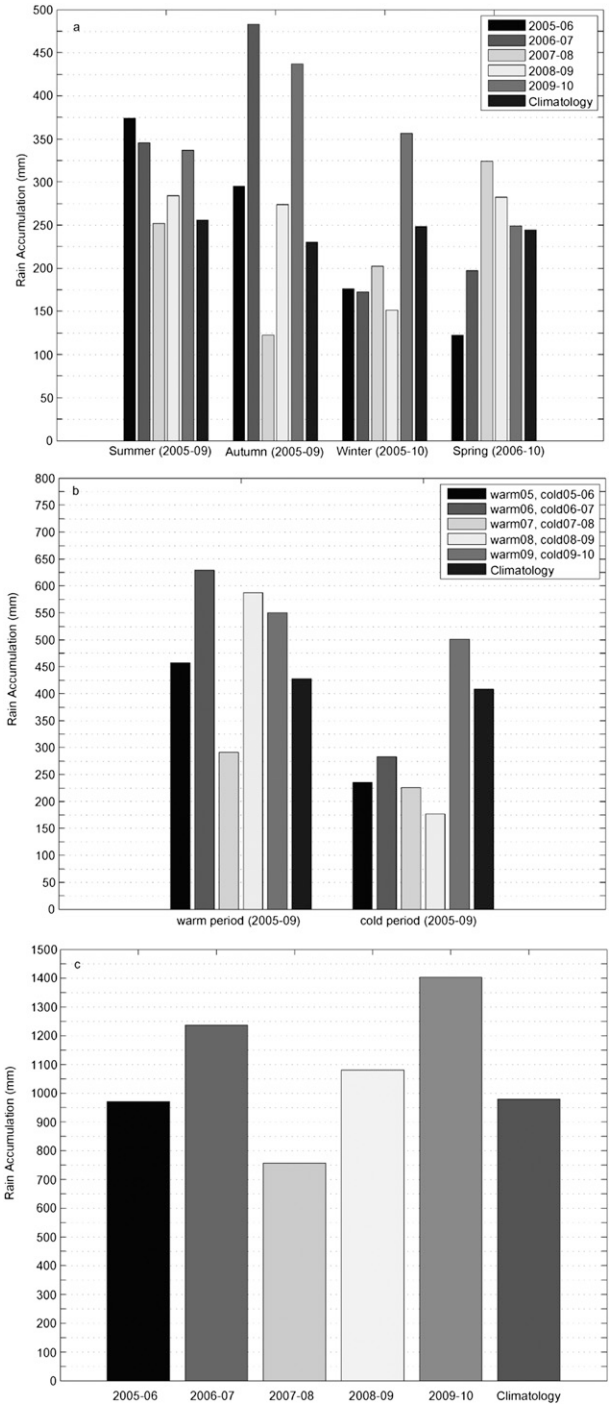

FIG. 3. Five years of rainfall totals for (a) a season, (b) warm/cold periods, and (c) a year at Wallops Island, VA. The climatology was based on historical precipitation records at Wallops Island.

annual totals were based on June through May. The spatial variability was also studied for four physically based events that included remnants of tropical cyclones, air mass convection, nor'easters, and frontal (warm sector) rainfall. The minimum sample size was 145 observations, which occurred during the winters of 2006/07 and 2007/08 (Fig. 4). The sample size can be enhanced by selecting a single tip for the rain/no-rain threshold, but a single tip can be the result of wind effects, and the time of the tip will not represent a rainy period in the presence of a partially filled bucket from a previous storm.

Pearson's correlation coefficient is applied to 55 pairs of gauge records. A three-parameter exponential function is then applied to the correlation r and distance d pairs for each integration period and is expressed as

$$r = r_0 \exp\left[-\left(\frac{d}{d_0}\right)^s\right], \tag{1}$$

where r_0 is the nugget parameter, d is the distance between the two gauge sites, d_0 is the correlation distance, and s is the shape parameter.

The nugget parameter is the correlation between the collocated gauges, and one of the sites at Wallops Flight Facility (WFF), Wallops Island, Virginia, was used to determine the nugget parameter. In an ideal case, the collocated gauges should result in a correlation coefficient of 1, but the random measurement errors and microscale variability of rainfall result in correlation coefficients mostly between 0.95 and 0.99 (TO12). We used these two predefined nugget parameters to investigate the importance of nuggets in determining the correlation distance and shape parameter. The correlation distance and shape parameter are determined by minimizing the root-mean-square error (rmse) between the correlations in Eq. (1) and those directly calculated from a pair of observations. The shape parameter controls the behavior of the exponential function at small separation distances and was mainly between 0.5 and 1.0 in the TO12 study. A shape parameter of 1 results in exponential decay of the correlation, while a shape parameter of 0.5 shows faster exponential decay at shorter separation distances and slower exponential decay at longer separation distances. At crossover between shorter and longer separation distances, $d = d_0$ and $r = r_0/e$. We used these two predefined shape parameters to investigate the role of the shape parameter in determining correlation distance.

5. Spatial variability

For the entire observational period, the correlations fell below 0.5, 0.2, and 0.1 at 10-, 40-, and 80-km distances, respectively (Fig. 5). Most of the paired correlations were between 20- and 60-km distance, and the maximum difference in correlation at a given distance was less than 0.15. The nugget parameter calculated from collocated gauges was 0.93. The correlation distance and the shape parameter were 17.2 km and 0.57, respectively, for the exponential fit. The rmse, which shows the goodness of the fit, was 0.04.

For the seasons, the year-to-year variations of the correlations were substantial during autumn and spring. At 20-km distance, the correlations were between 0.3 and 0.6 during spring and between 0.3 and 0.52 during autumn (Figs. 6a,c). The year-to-year variability was relatively less during summer, and the correlations fell below 0.1 at 50-km distance (Fig. 6b). The year-to-year variability was also low during winter, but the correlations remained higher than 0.1, even at 150 km (Fig. 6d).

The correlations were less than 0.2 and 0.1 at 40 and 80 km, respectively, during the warm period (Fig. 7a) and higher than 0.2 and 0.1 at 90 and 150 km, respectively, during the cold period (Fig. 7b). The drastic differences in correlations between the cold and warm periods show the dependence of rainfall variability on the precipitation systems. On an annual basis, the correlations were less than 0.4 and 0.2 at 20 and 60 km, respectively (Fig. 7c).

Considering the variability of rainfall for different precipitation systems, the correlations fell below 0.1 at 40-km distance in air mass convection. At the same distance, the correlations were just below 0.3 in tropical cyclones, 0.4 in frontal precipitation, and just above 0.5 in nor'easters (Fig. 8). The precipitation systems were determined through synoptic charts on an event-by-event basis. A close agreement in correlation distance between air mass convection and summer season, and between the nor'easters and winter season, shows the dominance of weather systems on seasonal precipitation.

The integration period and rain/no-rain threshold has a pronounced effect on the quantitative analysis of the rainfall variability (Ciach and Krajewski 2006; Villarini et al. 2008). At 40-km distance, a single- and an eight-tip-based rain/no-rain threshold resulted in correlations of 0.25 and 0.12, respectively (Fig. 9a). The higher rain/no-rain thresholds eliminate the light rain and therefore lower the correlations between the paired gauge measurements. The correlations were 0.05 and 0.65 at 40-km distance when 5-min and 12-h integration periods were considered (Fig. 9b).

6. Parameters of exponential fit

The nugget parameter was mostly higher than 0.95 for any given time period or weather system considered

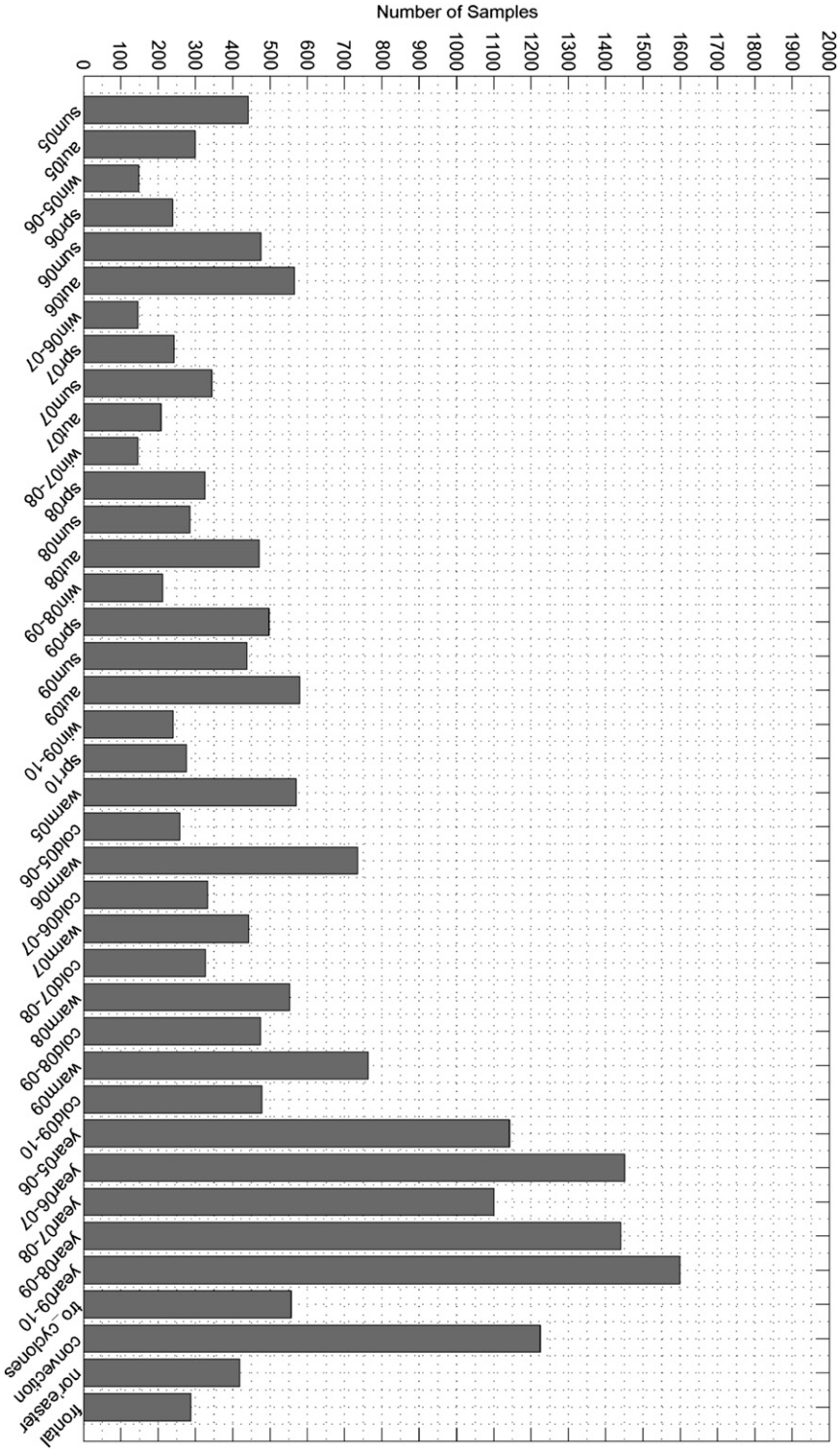

FIG. 4. Sample size for a given season, warm/cold periods, years, and specific weather types.

(Fig. 10a). At the same time, the nugget was 0.85, its lowest value, during the spring of 2006. The shape parameter was usually between 0.4 and 1.0 but was as high as 2.0 during the winter of 2008/09 and as low as 0.2 during the spring of 2010 (Fig. 10b). The predefined nugget parameter-based exponential fits resulted in insignificant differences in the shape parameter. The maximum difference in shape parameter was 0.15, which

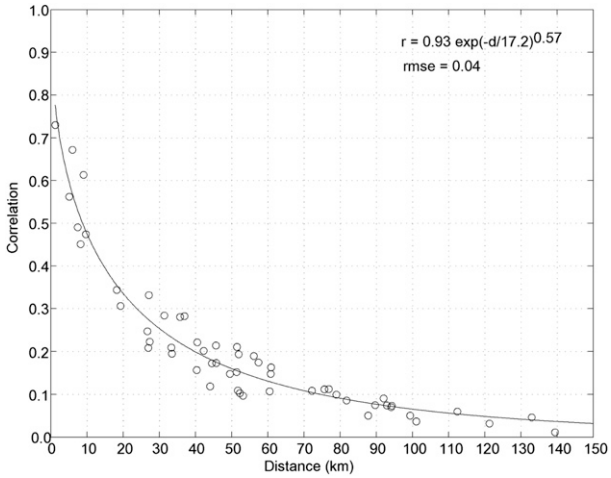

FIG. 5. Intergauge correlations (circles) and the fitted exponential function (curve) for 30-min time averaging. The parameters of the exponential function and rmse are also given.

occurred during the summer of 2007, when the best nugget parameter was 0.88.

The correlation distances were less than 20 km during summer and above 50 km during winter (Figs. 10c,d). During spring, the correlation distances had a wide range of year-to-year variability between 10 and 45 km, while the variability was relatively less during autumn, with a correlation distance range between 25 and 45 km. The correlation distances were 20–30 km during warm periods and at and above 50 km during cold periods. The yearly correlations lay between 20 and 30 km. Considering all climatological periods, the shortest and the longest correlation distances were 10 and 130 km, which were observed during the spring of 2006 and the 2009/10 cold period. The correlation distances were 15 and 30 km during air mass convection and tropical cyclones, respectively, while they were 55 and 80 km during frontal rainfall and nor'easters, respectively. The correlation distances are relatively less sensitive to the nugget parameter than the shape parameter (Figs. 10c,d). This demonstrates that a predefined nugget parameter may be considered to determine the correlation distance in the absence of collocated gauge. The shape parameter, on the other hand, should be retrieved from three-parameter exponential function.

The short correlation distance of air mass convection also occurred during the summers of 2005, 2006, and

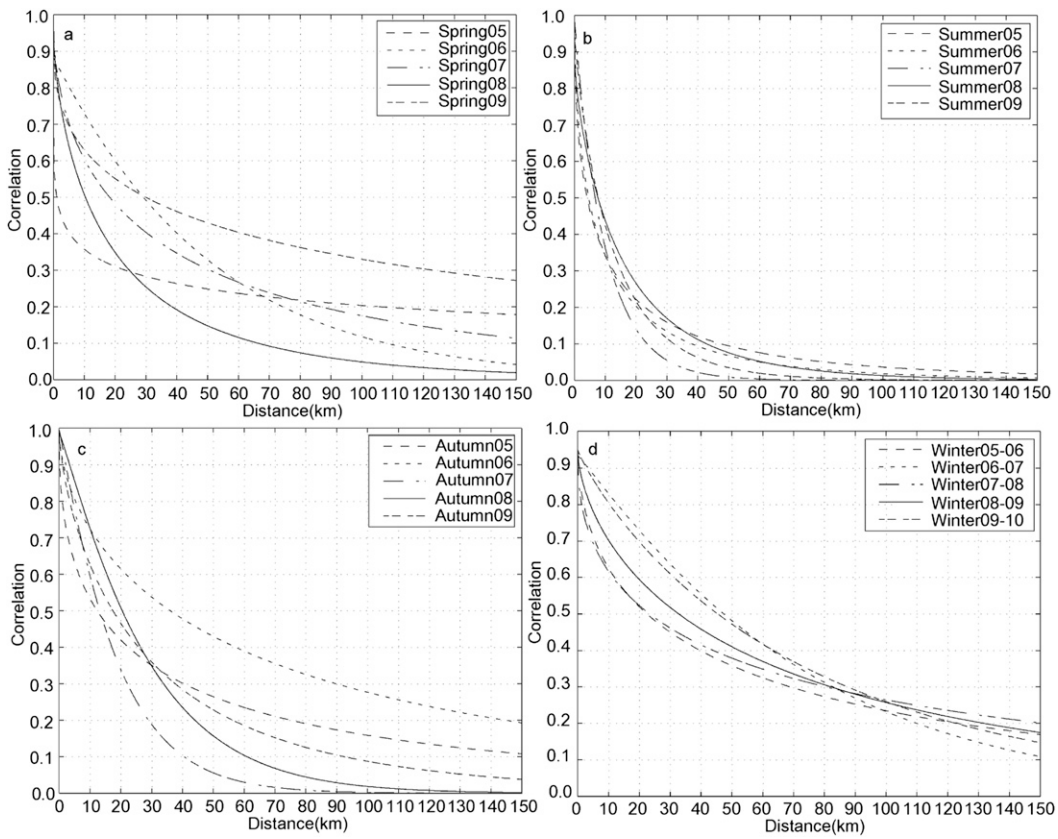

FIG. 6. Correlation of functional fit for five consecutive years for (a) spring, (b) summer, (c) autumn, and (d) winter seasons.

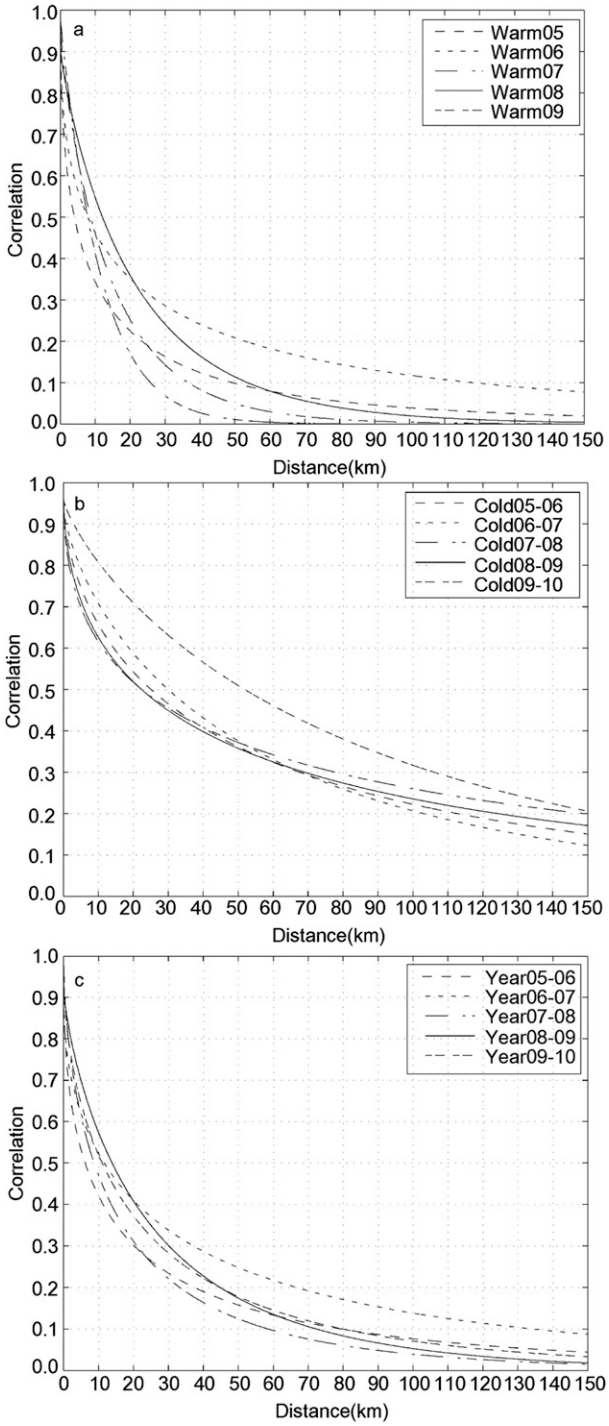

FIG. 7. Correlation of functional fit for five consecutive years for (a) warm period, (b) cold period, and (c) entire year.

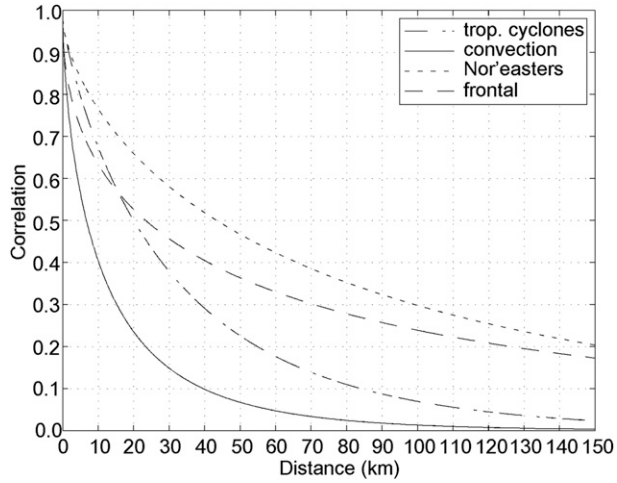

FIG. 8. Correlation of functional fit for four different weather systems.

2007. Similarly, the correlation distances of tropical cyclones were observed during the autumns of 2005, 2008, and 2009. The high correlation distances of nor'easters were also examined during the winters of 2006/07, 2008/09, and 2009/10. These observations show how a particular weather system can dominate the spatial variability of rainfall in a season. In particular, a season for which no tropical cyclone is observed will result in a different correlation distance than in a season where one or more tropical cyclones occur. This shows the necessity of a multiyear dataset to determine the spatial variability where the region is subject to different weather systems.

Considering the entire observational period, the nugget parameter increased with longer integration periods, and the increase in nugget was relatively faster at short integration periods (Fig. 11a). This shows that the gauge-to-gauge variability was more pronounced at shorter time periods. The shape parameter was between 0.52 and 0.56 up to 20-min integration, then increased with longer integration periods from 0.59 at 30-min to 0.66 at 3-h integration and was around 0.58 for 6- and 12-h integration periods (Fig. 11b). The correlation distance increased with longer integration period, first gradually, from 2 km at 5-min integration to 38 km at 1-h integration, and then rapidly, from 58 km at 2-h integration to 178 km at 12-h integration (Fig. 11c). The rmse was less than 0.05 up to 30-min integration period but then increased up to 0.88 at 12-h integration (Fig. 11d).

7. Conclusions

An experimental study of spatial variability of rainfall was conducted using a high-quality rain gauge network on the Delmarva Peninsula. This study is aimed at quantifying the rainfall variability within the IFOV of typical satellite microwave sensors. The variability within the IFOV results in nonuniform beam filling, which is one of key uncertainties in the microwave

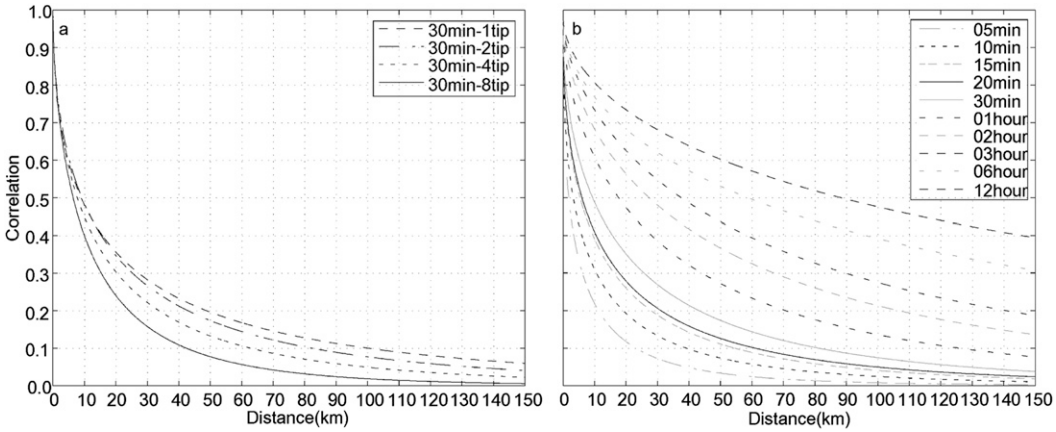

FIG. 9. Correlation of functional fit for (a) four different rain/no-rain thresholds and (b) 10 different integration periods.

sensor–based precipitation estimate. Rain gauge observations over a 5-yr period provided the data to investigate the variability over different time periods and four specific weather systems. The spatial variability was more pronounced at smaller separation distances as the correlations fell below 0.5 at 10-km distance for the experiment period at 30-min time integration. The correlations gradually decreased from 0.3 to 0.1 between 30 and 80 km and remained less than 0.1 for longer separation distances.

A sharp decay in correlations at shorter separation distances was particularly pronounced during summer and warm periods while the correlations had a more gradual decay during winter and cold periods. The correlations had pronounced differences from one year to the next during spring and autumn. Significant differences in correlations were also observed between the four weather systems. The nor'easters had more uniform precipitation followed by frontal precipitation. The tropical cyclones and air mass convection exhibited high spatial variability, resulting in lower correlations at a given distance. The correlation distances during summers and during air mass convection were about the same, indicating the dominance of air mass convection during summer in this region. Similarly, nor'easters resulted in higher correlation distances during winter. The correlations increased with longer integration periods and lower rain/no-rain thresholds.

The three-parameter exponential function had a very good fit to the observed correlations. The differences between observed correlations and the fitted curve were very small, and there was at least one paired correlation every 10 km of distance. The rmse was therefore 0.25 or less for any season, warm/cold, and yearly periods. The nugget parameter, which is the correlation of collocated gauges, was higher than 0.95 in most of the observational periods, but it was as low as 0.85 during the spring of 2006. The gauge measurement errors and variability between the collocated rain gauges contributed to the deviation of nugget parameter from one. The shape parameter of the exponential fit ranged mostly from 0.4 to 1.0. The correlation distance of the exponential fit had a wide range but was between 8 and 13 km during summer and between 51 and 67 km during winter. The correlation distance showed more sensitivity to the shape parameter than the nugget parameter.

8. Future research

The correlation distance is the measure of the spatial variability of rainfall and is one of the key parameters in designing a gauge network for validating satellite precipitation estimates. As shown in this study, the correlation distance is sensitive to the integration period, rain/no-rain threshold, precipitation characteristics, and the size and gauge density of the domain. The microwave sensors, for instance, have a wide range of IFOV depending on their frequency of operation, and therefore, an additional rain gauge network is needed to detect the rainfall variability at shorter distances.

To achieve these goals, six triple-gauge sites have been added to the network, and a new network in Pocomoke City, Maryland, where 25 dual gauges are deployed within a $5 \times 5\,\mathrm{km}^2$ array, will be used to study the small-scale variability of rainfall. The new network will replace the three gauge sites at Wallops Island. The upgraded gauge network will provide additional paired correlations at various distances. Thus, the shape parameter and correlation distance of the exponential function will be more accurate. The upgraded network

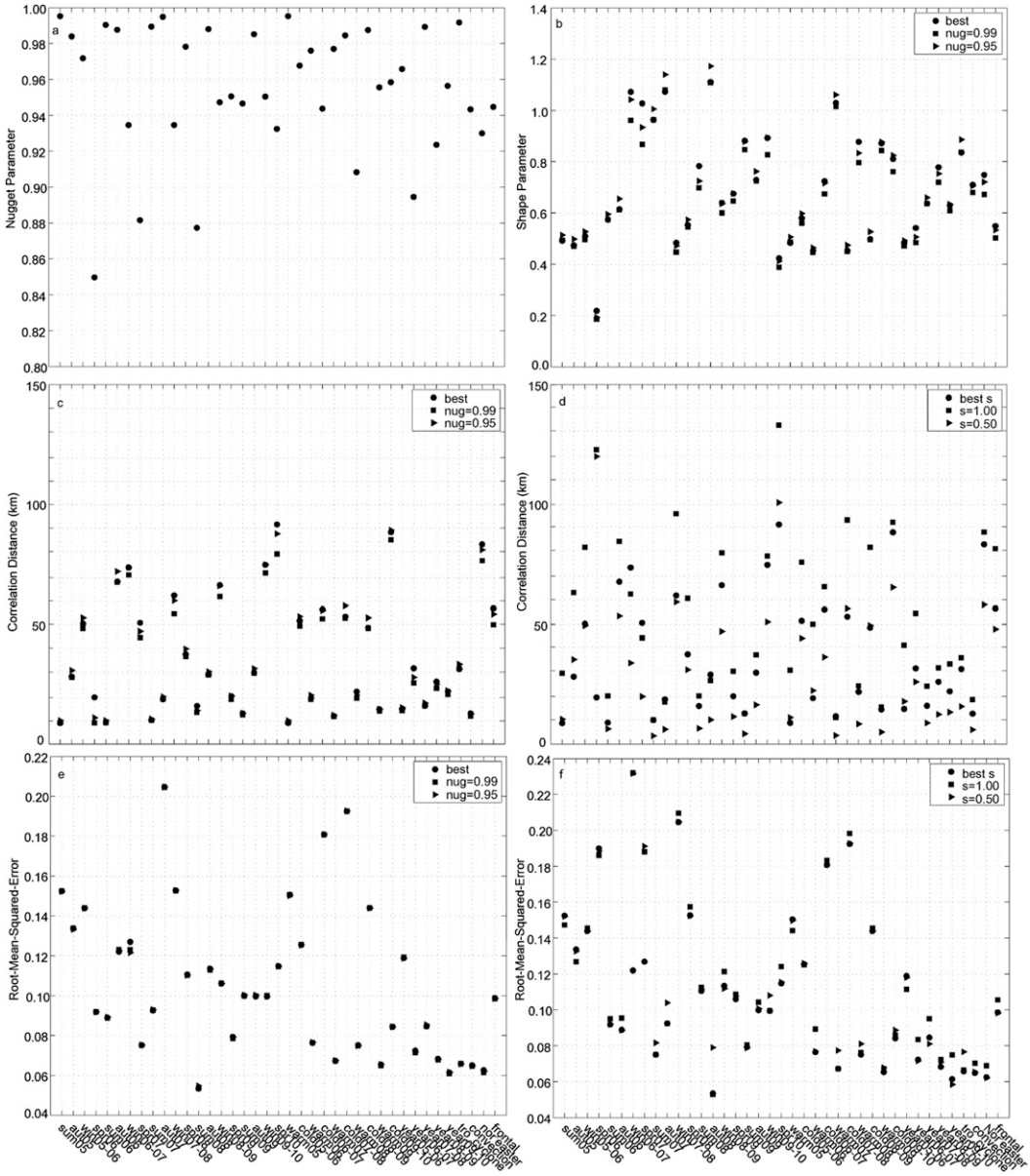

FIG. 10. Parameters of exponential fit and rmse for 20 seasons, 10 warm/cold periods, 5 yr, and for tropical cyclones, air mass convection, nor'easters, and frontal systems: (a) nugget parameter; (b) shape parameter; (c) correlation distance for the best and selected nugget parameters; (d) as in (c), but for selected shape parameters; (e) rmse for the best and selected nugget parameters; and (f) as in (e), but for selected shape parameters.

and the longer dataset will provide more robust estimates of the correlation distances from the four major weather systems in the mid-Atlantic region.

The upgraded gauge network will be used to evaluate the satellite precipitation products, especially after launch of the GPM satellite. The microwave sensor–based precipitation estimates perform relatively poorly over land and coastal regions. There have been efforts to merge gauge rainfall with the satellite products. Vila et al. (2009), for instance, showed an improvement in TMPA over South America when daily gauge reports merged with this product. The upgraded gauge network on the Delmarva Peninsula will serve as an excellent dataset to develop merged gauge satellite precipitation products at the time resolution of the satellite product.

It should be added that the dense gauge networks are not the only resource that can be used to investigate spatial variability within the IFOV. The National Oceanic and Atmospheric Administration National Severe Storm Laboratory's ground-based National Mosaic

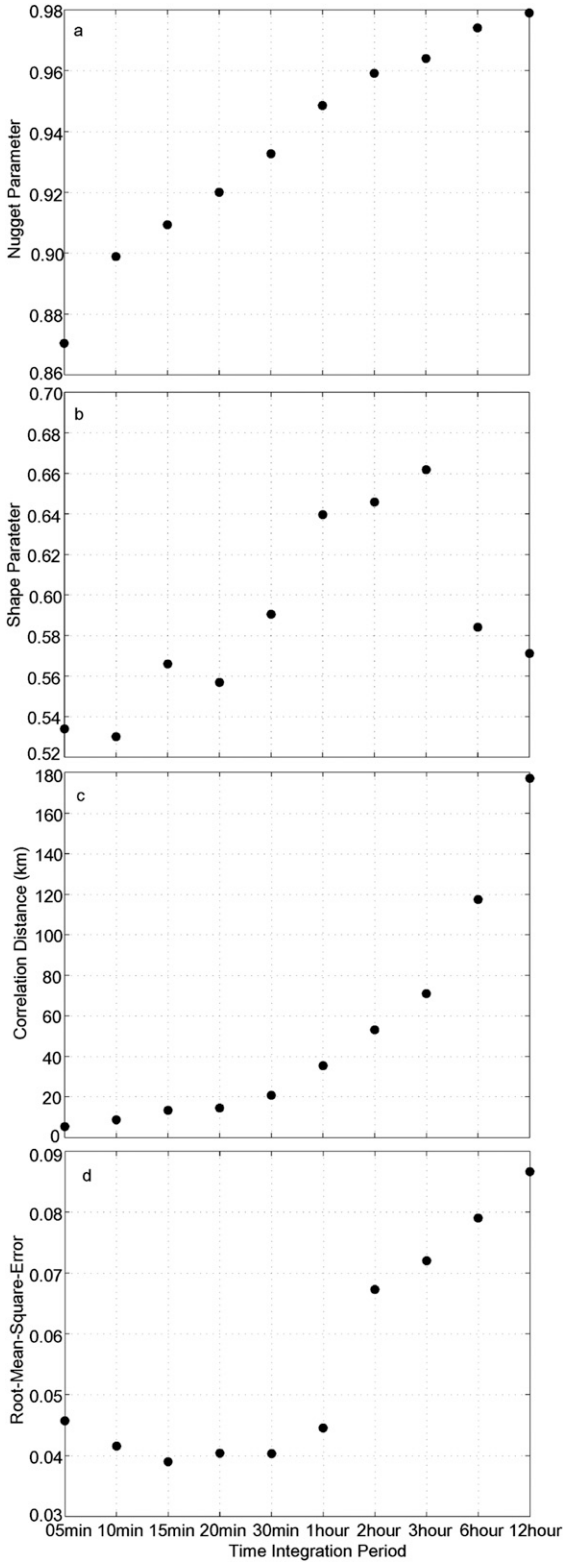

FIG. 11. Dependence of (a) nugget parameter, (b) correlation distance, (c) shape parameter of the exponential function, and (d) rmse on the averaging time scale ranging from 5 min to 12 h.

and Multi-Sensor Quantitative Precipitation Estimation (NMQ/Q2) system (Zhang et al. 2011) produces gauge-adjusted, radar-based precipitation products at 0.01° spatial resolution over the continental United States. This product was recently used to evaluate the TRMM precipitation radar rainfall estimate (Kirstetter et al. 2013). The gauge network used in this study is not part of the NMQ/Q2 product and therefore can be used to evaluate the NMQ/Q2 product. The NMQ/Q2 product itself is a candidate to determine the spatial variability across the United States.

Acknowledgments. The second author was a summer intern under NASA's Water Escapes program; Fernando Miralles of Florida International University is the principal investigator. Acknowledgements extend to Robert Meneghini of the NASA Goddard Space Flight Center and S. Joseph Munchak of the University of Maryland for their valuable comments. Special thanks to Joseph Turk, Editor of the *Journal of Hydrometeorology*, for his guidance throughout the review process. We are also thankful for the constructive comments from the anonymous reviewers. This study was funded under NASA's Global Precipitation Measurement Mission under Arthur Hou, project scientist, NASA Goddard Space Flight Center, and the Precipitation Measurement Mission (PMM) NNX07AF45G and NNX10AJ12G under Ramesh Kakar, program scientist, NASA Headquarters. Acknowledgments extend to Mathew Schwaller, GPM ground validation manager, NASA Goddard Space Flight Center, for his continuous support.

REFERENCES

Aonashi, K., and Coauthors, 2009: GSMaP passive, microwave precipitation retrieval algorithm: Algorithm description and validation. *J. Meteor. Soc. Japan,* **87A,** 119–136, doi:10.2151/jmsj.87A.119.

Berndtsson, R., 1987: On the use of cross-correlation analysis in studies of patterns of rainfall variability. *J. Hydrol.,* **93,** 113–134, doi:10.1016/0022-1694(87)90198-3.

Bewket, W., and D. Conway, 2007: A note on the temporal and spatial variability of rainfall in the drought-prone Amhara region of Ethiopia. *Int. J. Climatol.,* **27,** 1467–1477, doi:10.1002/joc.1481.

Ciach, G. J., and W. F. Krajewski, 2006: Analysis and modeling of spatial correlation structure in small-scale rainfall in central Oklahoma. *Adv. Water Resour.,* **29,** 1450–1463, doi:10.1016/j.advwatres.2005.11.003.

Gebremichael, M., and W. F. Krajewski, 2004: Assessment of the statistical characterization of small-scale rainfall variability from radar: Analysis of TRMM ground validation datasets. *J. Appl. Meteor.,* **43,** 1180–1199, doi:10.1175/1520-0450(2004)043<1180:AOTSCO>2.0.CO;2.

Habib, E., and W. F. Krajewski, 2002: Uncertainty analysis of the TRMM ground-validation radar-rainfall products: Application

to the TEFLUN-B field campaign. *J. Appl. Meteor.,* **41,** 558–572, doi:10.1175/1520-0450(2002)041<0558:UAOTTG>2.0.CO;2.

Huffman, G., and Coauthors, 2007: The TRMM Multisatellite Precipitation Analysis (TMPA): Quasi-global, multiyear, combined-sensor precipitation estimates at fine scales. *J. Hydrometeor.,* **8,** 38–55, doi:10.1175/JHM560.1.

Joyce, J. R., E. J. Janowiak, P. A. Arkin, and P. Xie, 2004: CMORPH: A method that produces global precipitation estimates from passive microwave and infrared data at high spatial and temporal resolution. *J. Hydrometeor.,* **5,** 487–503, doi:10.1175/1525-7541(2004)005<0487:CAMTPG>2.0.CO;2.

Kirstetter, P. E., Y. Hong, J. J. Gourley, M. Schwaller, W. Petersen, and J. Zhang, 2013: Comparison of TRMM 2A25 products, version 6 and version 7, with NOAA/NSSL ground radar-based national mosaic QPE. *J. Hydrometeor.,* **14,** 661–669, doi:10.1175/JHM-D-12-030.1.

Mandapaka, P. V., W. F. Krajewskia, G. J. Ciacha, G. Villarinia, and J. A. Smith, 2009: Estimation of radar-rainfall error spatial correlation. *Adv. Water Resour.,* **32,** 1020–1030, doi:10.1016/j.advwatres.2008.08.014.

Moreau, E., J. Testud, and E. Le Bouar, 2009: Rainfall spatial variability observed by X-band weather radar and its implication for the accuracy of rainfall estimates. *Adv. Water Resour.,* **32,** 1011–1019, doi:10.1016/j.advwatres.2008.11.007.

Tokay, A., and K. Öztürk, 2012: An experimental study of small-scale variability of rainfall. *J. Hydrometeor.,* **13,** 351–365, doi:10.1175/JHM-D-11-014.1.

——, P. G. Bashor, and V. L. McDowell, 2010: Comparison of rain gauge measurements in mid-Atlantic region. *J. Hydrometeor.,* **11,** 553–565, doi:10.1175/2009JHM1137.1.

Vila, D. A., L. G. Goncalves, D. L. Toll, and J. R. Rozante, 2009: Statistical evaluation of combined daily gauge observations and rainfall satellite estimates over continental South America. *J. Hydrometeor.,* **10,** 533–543, doi:10.1175/2008JHM1048.1.

Villarini, G., 2010: Evaluation of the research-version TMPA rainfall estimate at its finest spatial and temporal scales over the Rome metropolitan area. *J. Appl. Meteor. Climatol.,* **49,** 2591–2602, doi:10.1175/2010JAMC2462.1.

——, P. V. Mandapaka, W. F. Krajewski, and R. J. Moore, 2008: Rainfall and sampling uncertainties: A rain gauge perspective. *J. Geophys. Res.,* **113,** D11102, doi:10.1029/2007JD009214.

Zhang, J., and Coauthors, 2011: National Mosaic and Multi-sensor QPE (NMQ) system: Description, results, and future plans. *Bull. Amer. Meteor. Soc.,* **92,** 1321–1338, doi:10.1175/2011BAMS-D-11-00047.1.